Supporting Information for

A folded mechanochromic organic fluorophore based on thianthrene-fused coumarin

Masafumi Ueda*, Asuka Uehara, Kazuteru Usui, and Masashi Hasegawa

1. Experimental Procedures

General

All the reagents used were commercially sourced. Column chromatography was carried out using a KANTO CHEMICAL silica gel 60 N (spherical, neutral, 63-210 μm). Melting points were determined using a Yanaco MP-500P micro melting point apparatus. ^{1}H, ^{13}C, and ^{19}F NMR spectra were recorded using a Bruker AVANCE 400 instrument and JEOL JNM-ECZ 600 NMR spectrometer (^{1}H frequency: 400 and 600 MHz; ^{13}C frequency: 100 and 150 MHz; ^{19}F frequency: 376 MHz). Chemical shifts were recorded in ppm, and *J* values were recorded in Hz. The data are reported in ppm and referenced to the internal reference standard tetramethylsilane (Me_4Si) for proton and carbon, trichlorofluoromethane (C_6H_5F) for fluorine. The residual signals of the NMR solvents used were 7.26 ppm (proton for $CDCl_3$), 77.16 ppm (carbon for $CDCl_3$), and −113.15 ppm (fluorine for C_6H_5F). The following abbreviations are used to denote multiplicities: s (singlet), d (doublet), t (triplet), q (quartet), dd (double doublet), and m (multiplet). HRMS spectra were recorded on a Thermo Scientific Exactive Plus Orbitrap mass spectrometer for ionization. Only intense or structurally diagnostic mass spectral fragment ion peaks are reported.

X-ray Crystallography

Diffraction data were collected using a Rigaku XtaLAB Synergy-S system with a multilayer mirror-monochromatized Cu*K*a radiation (λ = 1.54184 Å) at Kitasato University. The raw frame data were integrated via the CrysAlisPro software package[S1]. Using Olex2[S2], the crystal structures were solved by employing SHELXT[S3] and refined using full-matrix least squares in F^2 (SHELXL)[S4]. Hydrogen atoms were introduced at the calculated position included in the structure factor calculation but were not refined. The figures were generated from images displayed via the Mercury software package. Powder X-ray diffraction (XRD) patterns were recorded on a Rigaku SmartLab.

Spectroscopic Studies

UV-vis spectra were recorded using a JASCO V560 instrument. Fluorescence spectra were collected using a JASCO FP-8550 spectrofluorometer. The fluorescence quantum yields were determined using a JASCO ILF-135|120 mm dia. Φ integrating Sphere. Fluorescence lifetimes were measured using a HORIBA FluoroCube. The fluorescence decay curves of 6,7-BDTC were recorded using the Time-Correlated Single Photon Counting (TCSPC) method. The excitation wavelength was 378 nm. Solution samples were measured using a quadruple clear quartz cell, while solid samples were measured by sandwiching powder and crystals between cover glasses. The fluorescence decay curves obtained from the measurements were corrected using the Instrument Response Function (IRF). For solution samples, aqueous colloidal silica was used as a scatterer for correction, and for solid samples, cover glass was used for similar correction.

Quantum Chemical Calculations

All calculations were performed with the Gaussian 16 software package (Revision C.01)[S5] at the Research Center for Computational Science (Okazaki, Japan). The optimized structures, theoretical spectra, and electronic transitions were estimated using spin-restricted density functional theory (DFT) with the CAMB3LYP functional and the 6-31G(d,p) basis set. Vibration frequency calculations confirmed that all optimized structures correspond to real minima without any imaginary frequencies. The figures were generated via images from the Avogadro (ver. 1.2.0) software package.

Synthesis of **2**

In a 200 mL three-necked recovery flask, compound **1** (700 mg, 4.86 mmol) and CH_2Cl_2 (5 mL)

were mixed, and the mixture was cooled to 0 °C. A CH_2Cl_2 solution of $TiCl_4$ (1.0 M, 8.1 mL, 8.12 mmol) and then dichloromethylmethylether (0.44 mL, 4.86 mmol) was slowly added and stirred overnight at ambient temperature. The reaction was quenched with ice, extracted with CH_2Cl_2, washed with brine, and dried over anhydrous Na_2SO_4. The organic layer was concentrated under reduced pressure, and the residue was purified by column chromatography on silica gel using CH_2Cl_2 to yield compound **2** (452 mg, 2.63 mol) as a colorless oil in 54% yield.
^{1}H NMR (400 MHz, $CDCl_3$) δ 10.18 (d, *J* = 2.8 Hz, 1H), 7.46 (dd, *J* = 9.2 and 10.0 Hz, 1H), 6.74 (dd, *J* = 6.0 and 11.6 Hz, 1H), 3.83 (s, 3H).
^{13}C NMR (100 MHz, $CDCl_3$) δ 187.2, 158.8 (dd, *J* = 2.0 and 9.0 Hz), 155.0 (dd, *J* = 15.0 and 257 Hz), 145.2 (dd, *J* = 14.0 and 243 Hz), 121.4–121.1 (m), 116.3 (dd, *J* = 3.0 and 18.0 Hz), 101.9 (d, *J* = 22.0 Hz), 56.6.
^{19}F NMR (376 MHz, $CDCl_3$) δ −123.42 - −123.66 (m), −146.53 - −147.14 (m)
HRMS (ESI, positive mode): *m/z* calcd for $C_8H_7O_2F_2$ $[M+H]^+$ 173.0409; found 173.0408.

Synthesis of **3**

In a 200 mL recovery flask, a mixture of compound **3** (303 mg, 1.76 mmol), ethyl(triphenylphosphoranylidene)acetate (689 mg, 1.98 mmol), and CH_2Cl_2 (30 mL) was stirred for 2 hr at 40 °C. Ethyl(triphenylphosphoranylidene)acetate (350 mg, 1.00 mmol) was additionally added to the reaction mixture and stirred for 3 hr at the same temperature. The reaction was quenched with water, extracted with CH_2Cl_2, and dried over anhydrous Na_2SO_4. After evaporation under reduced pressure, the residue was purified by column chromatography on silica gel using CH_2Cl_2 and EtOAc to afford compound **3** (348 mg, 1.61 mmol) as a mixture of *E*/*Z* forms (4:1) of colorless solid in 92% yield.
^{1}H NMR (400 MHz, $CDCl_3$) (*E*)-**3**: δ 7.64 (dd, *J* = 0.8 and 16.0 Hz, 1H), 7.11 (dd, *J* = 9.2 and 11.2 Hz, 1H), 6.57 (dd, *J* = 5.8 and 12.0 Hz, 1H), 6.21 (d, *J* = 16.0 Hz, 1H), 4.10 (q, *J* = 7.2 Hz, 2H), 1.18 (t, *J* = 7.2 Hz, 3H); (*Z*)-**3**: δ 7.51 (dd, *J* = 9.6 and 11.6 Hz, 1H), 6.85 (d, *J* = 12.8 Hz, 1H), 6.53 (dd, *J* = 10.8 and 12.4 Hz, 1H), 5.78 (d, *J* = 12.0 Hz, 1H), 4.01 (q, *J* = 7.2 Hz, 2H), 1.10 (t, *J* = 7.2 Hz, 3H).
^{13}C NMR (100 MHz, $CDCl_3$) (*E*)-**3**: δ 167.0, 154.8 (d, *J* = 7 Hz), 152.6 (dd, *J* = 16 and 251 Hz), 144.6 (dd, *J* = 13 and 240 Hz), 137.7, 119.8–119.5 (m), 119.4, 116.3 (d, *J* = 20 Hz), 101.2 (d, *J* = 21 Hz), 60.5, 56.3, 14.3; (*Z*)-**3**: δ 165.9, 154.0 (dd, *J* = 2 and 8 Hz), 150.9 (dd, *J* = 14 and 249 Hz), 143.8 (dd, *J* = 13 and 239 Hz), 136.7, 120.6, 120.0–119.8 (m), 119.3 (dd, *J* = 1 and 20 Hz), 100.3 (d, *J* = 21 Hz), 60.4, 56.3, 14.1.
^{19}F NMR (376 MHz, $CDCl_3$) (*E*)-**3**: δ −131.33 - −131.45 (m), −147.75 - −147.95 (m); (*Z*)-**3**: −132.8 - −133.3 (m), −148.6 - −149.1 (m)
HRMS (ESI, positive mode): *m/z* calcd for $C_{12}H_{13}O_3F_2$ $[M+H]^+$ 243.0827; found 243.0826.

Synthesis of **4**

In a 100 mL recovery flask, compound **3** (2.42 g, 11.2 mmol) and CH_2Cl_2 (40 mL) were mixed, and the mixture was cooled to 0 °C. A CH_2Cl_2 solution of BBr_3 (1.0 M, 2.6 mL, 28.0 mmol) was slowly added and stirred for 5 hr at 50 °C. After cooling to ambient temperature, the reaction was quenched with H_2O. The reaction mixture was extracted with CH_2Cl_2, washed with brine, and dried over anhydrous Na_2SO_4. The residue was concentrated under reduced pressure and purified by column chromatography on silica gel using CH_2Cl_2 to yield compound **4** (1.50 g, 8.23 mmol) as a colorless block in 73% yield.
^{1}H NMR (400 MHz, $CDCl_3$) δ 7.62 (d, *J* = 10.0 Hz, 1H), 7.30 (dd, *J* = 8.4 and 9.2 Hz, 1H), 7.17 (dd, *J* = 6.8 and 10.8 Hz, 1H), 6.42 (d, *J* = 9.6 Hz, 1H).
^{13}C NMR (100 MHz, $CDCl_3$) δ 159.7, 152.4 (dd, *J* = 14.0 and 255 Hz), 150.4 (d, *J* = 8.0 Hz), 147.4 (dd, *J* = 14.0 and 246 Hz), 142.0, 116.8 (d, *J* = 3.0 Hz), 106.5 (d, *J* = 21.0 Hz)
^{19}F NMR (376 MHz, $CDCl_3$) δ −128.46 - −128.67 (m), −140.80 - −140.90 (m)
HRMS (ESI, positive mode): *m/z* calcd for $C_9H_5O_2F_2$ $[M+H]^+$ 183.0252; 183.0253.

Synthesis of **6,7-BDTC**

In a 50 mL two-necked recovery flask, a mixture of compound **4** (90 mg, 0.49 mmol), 1,2-

benzenedithiol (102 mg, 0.49 mol), Cs_2CO_3 (353 mg, 1.08 mmol), and dry DMF (5 mL) was stirred under an argon atmosphere for 24 hr at 120 °C. After cooling to ambient temperature, the mixture was poured into 1.0 M HCl aq. The aqueous layer was extracted with CH_2Cl_2, and the combined organic layer was washed with H_2O and dried over $MgSO_4$. The organic layer was concentrated under reduced pressure. The residue was purified by column chromatography on silica gel using CH_2Cl_2 to yield 6,7-BDTC (93 mg, 0.33 mmol) as a colorless block in 67% yield.
Mp = 212–213 °C
^{1}H NMR (400 MHz, $CDCl_3$) δ 7.62 (d, *J* = 9.6 Hz, 1H), 7.54 (s, 1H), 7.51–7.46 (m, 2H), 7.44 (s, 1H), 7.30–7.27 (m, 2H), 6.40 (d, *J* = 9.6 Hz, 1H).
^{13}C NMR (100 MHz, $CDCl_3$) δ 160.0, 153.4, 142.3, 141.0, 134.7, 134.2, 131.4, 128.9, 128.9, 128.3, 128.2, 126.8, 118.4, 116.9, 116.6.
HRMS (ESI, positive mode): *m/z* calcd for $C_{15}H_8O_2S_2$ $[M]^+$ 283.9960; found 283.9961.

References

S1. CrysAlisPro: Data Collection and Processing Software Package; Rigaku Oxford Diffraction, Rigaku Corporation, Yarnton, UK 2019.

S2. O. V. Dolomanov, L. J. Nourhis, R. J. Gildea, J. A. K. Howard and H. Puschmann, *J. Appl. Cryst.* 2009, **42**, 339.

S3. G. M. Scheldrick, *Acta Cryst.* 2015, **A71**, 3.

S4. G. M. Scheldrick, *Acta Cryst.* 2015, **C51**, 3.

S5. M. J. Frisch, G. W. Trucks, H. B. Schlegel, G. E. Scuseria, M. A. Robb, J. R. Cheeseman, G. Scalmani, V. Barone, G. A. Peterson, H. Nakatsuji, X. Li, M. Caricato, A. V. Marenich, J. Bloino, B. G. Janesko, R. Gomperts, B. Mennucci, H. P. Hratchian, J. V. Ortiz, A. F. Izmaylov, J. L. Sonnenberg, D. Williams-Young, F. Ding, F. Lipparini, F. Egidi, J. Goings, B. Peng, A. Petrone, T. Henderson, D. Ranasinghe, V. G. Zakrzewski, J. Gao, N. Rega, G. Zheng, W. Liang, M. Hada, M. Ehara, K. Toyota, R. Fukuda, J. Hasegawa, M. Ishida, T. Nakajima, Y. Honda, O. Kitao, H. Nakai, T. Vreven, K. Throssell, J. A. Jr., Montgomery, J. E. Peralta, F. Ogliaro, M. J. Bearpark, J. J. heyd, E. N. Brothers, K. N. Kudin, V. N. Staroverov, T. A. Keith, R. Kobayashi, J. Normand, K. Raghavachari, A. P. Rendell, J. C. Burant, S. S. Iyenger, J. Tomasi, M. Cossi, J. M. Millam, M. Klene, C. Adamo, R. Cammi, J. W. Ochterski, R. L. Martin, K. Morokuma, O. Farkas, J. B. Foresman and D. J. Fox, Gaussian 16 (Revision C.02) Gaussian Inc., Wallingford Ct, USA, 2016.

2. ^{1}H, ^{13}C, and ^{19}F NMR Charts

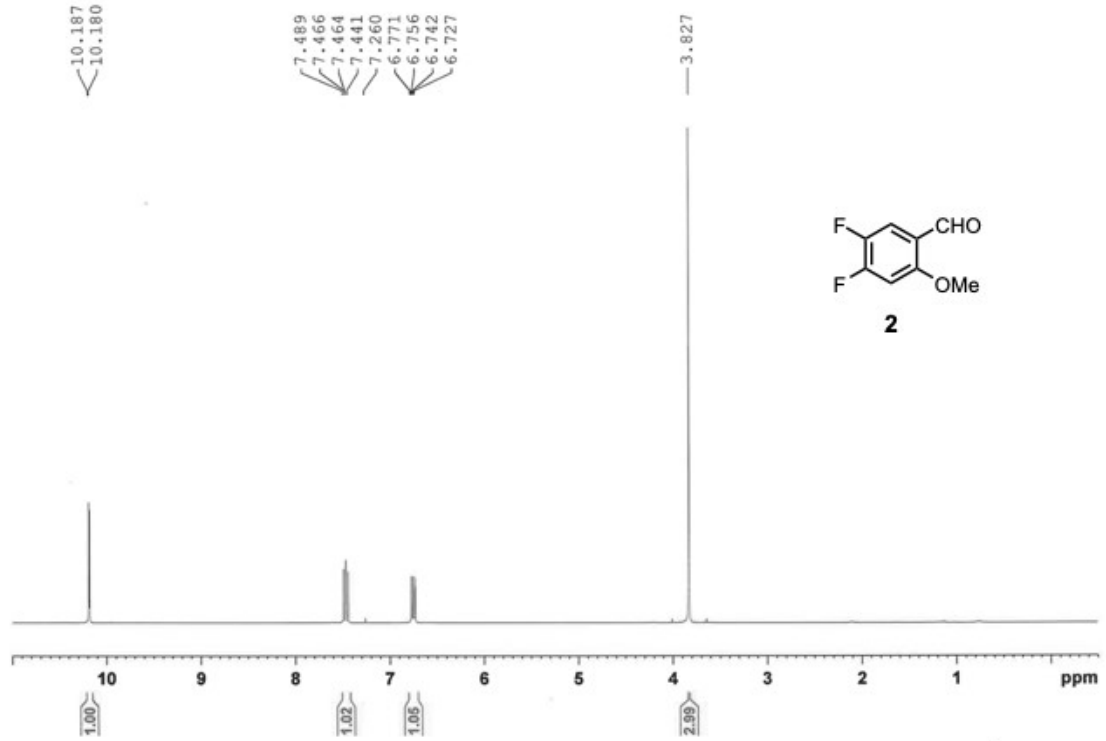

Figure S1. ^{1}H NMR spectrum of **2** ($CDCl_3$, 400 MHz)

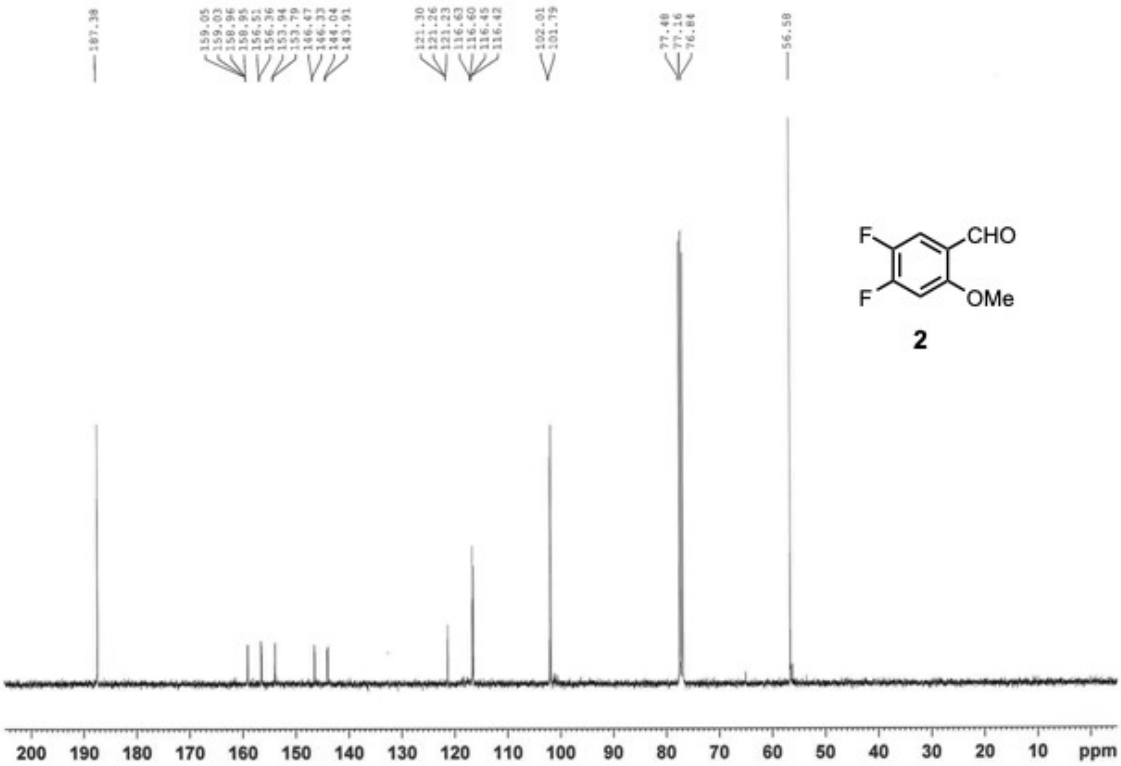

Figure S2. ^{13}C NMR spectrum of **2** ($CDCl_3$, 100 MHz).

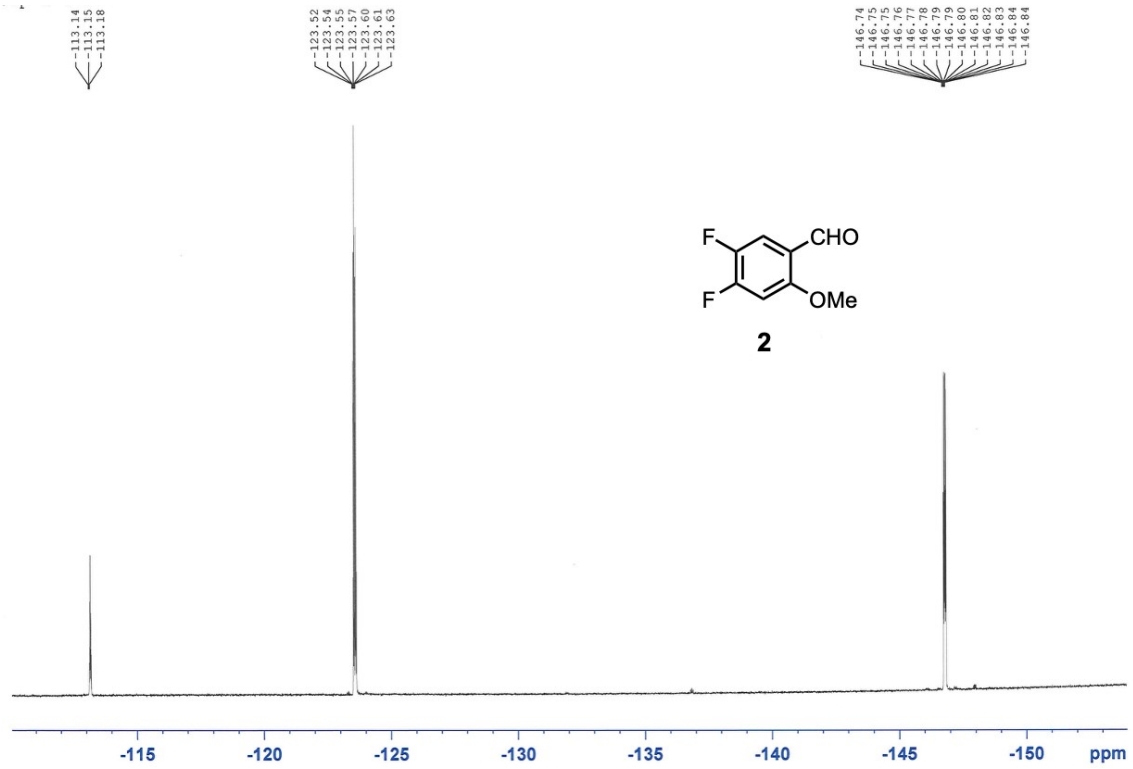

Figure S3. ^{19}F NMR spectrum of **2** ($CDCl_3$ with C_6H_5F, 376 MHz).

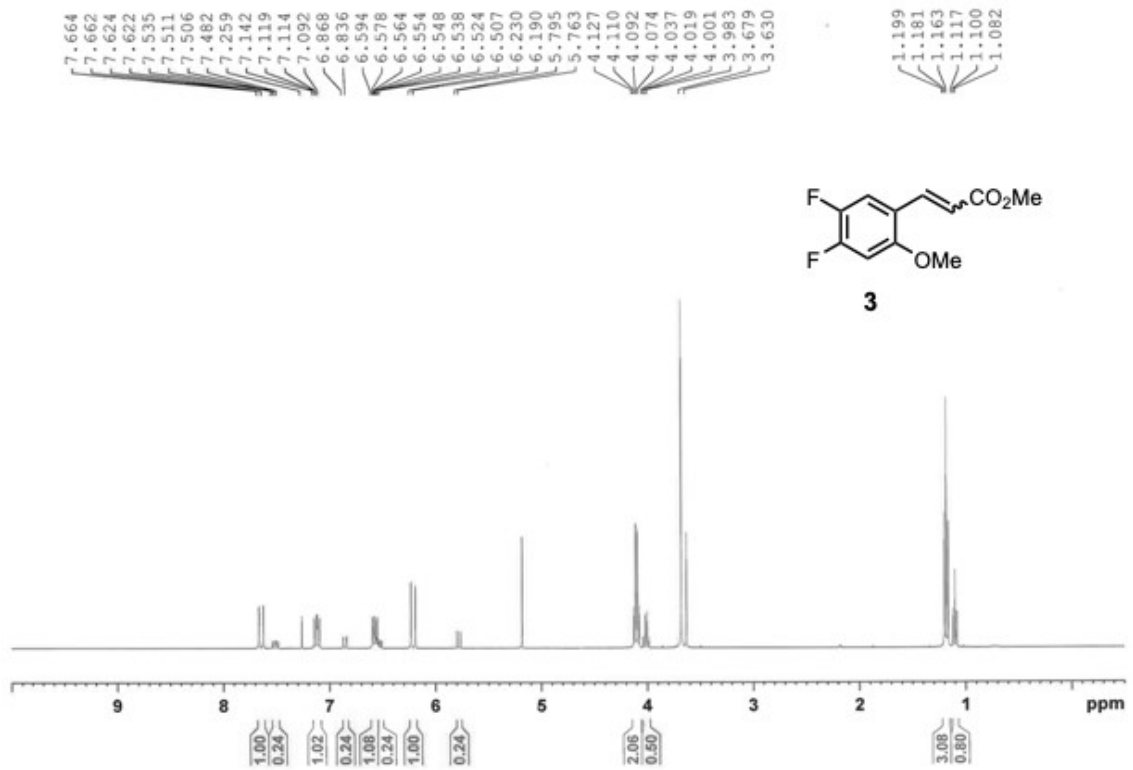

Figure S4. ^{1}H NMR spectrum of **3** (*E*/*Z* mixtures, $CDCl_3$, 400 MHz).

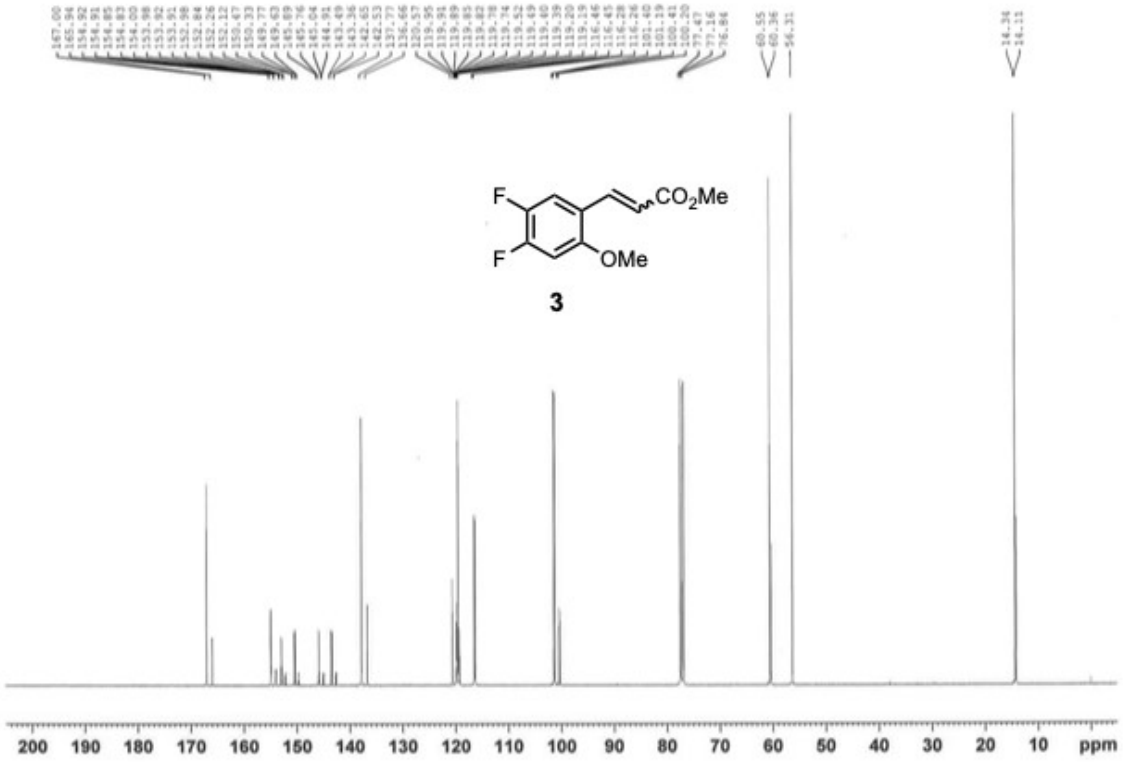

Figure S5. ^{13}C NMR spectrum of **3** (*E*/*Z* mixtures, $CDCl_3$, 100 MHz).

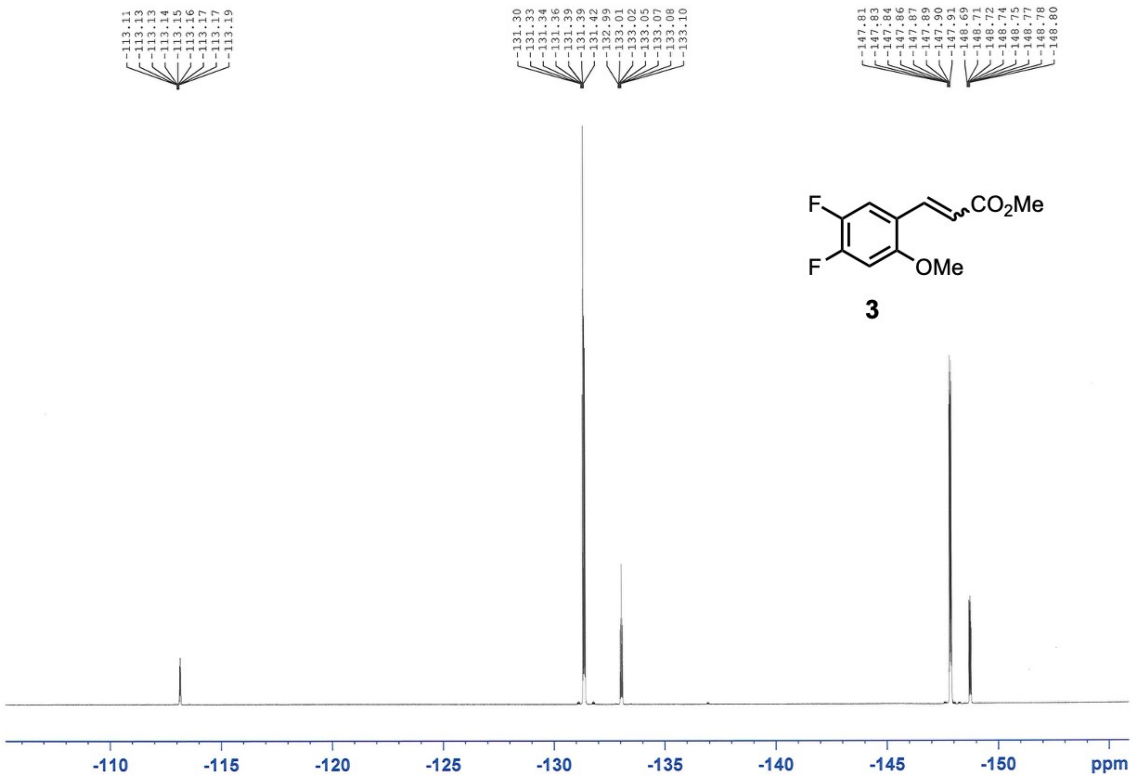

Figure S6. ^{19}F NMR spectrum of **3** (*E*/*Z* mixtures, $CDCl_3$ with C_6H_5F, 376 MHz).

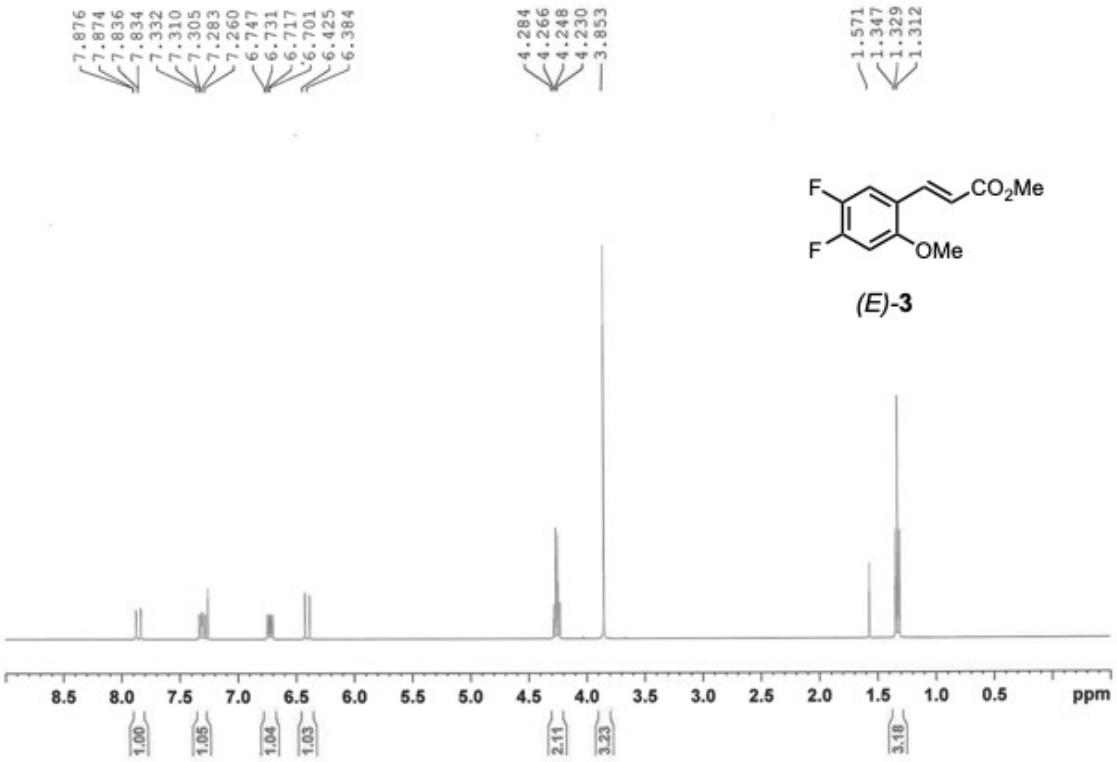

Figure S7. ^{1}H NMR spectrum of (*E*)-**3** ($CDCl_3$, 400 MHz).

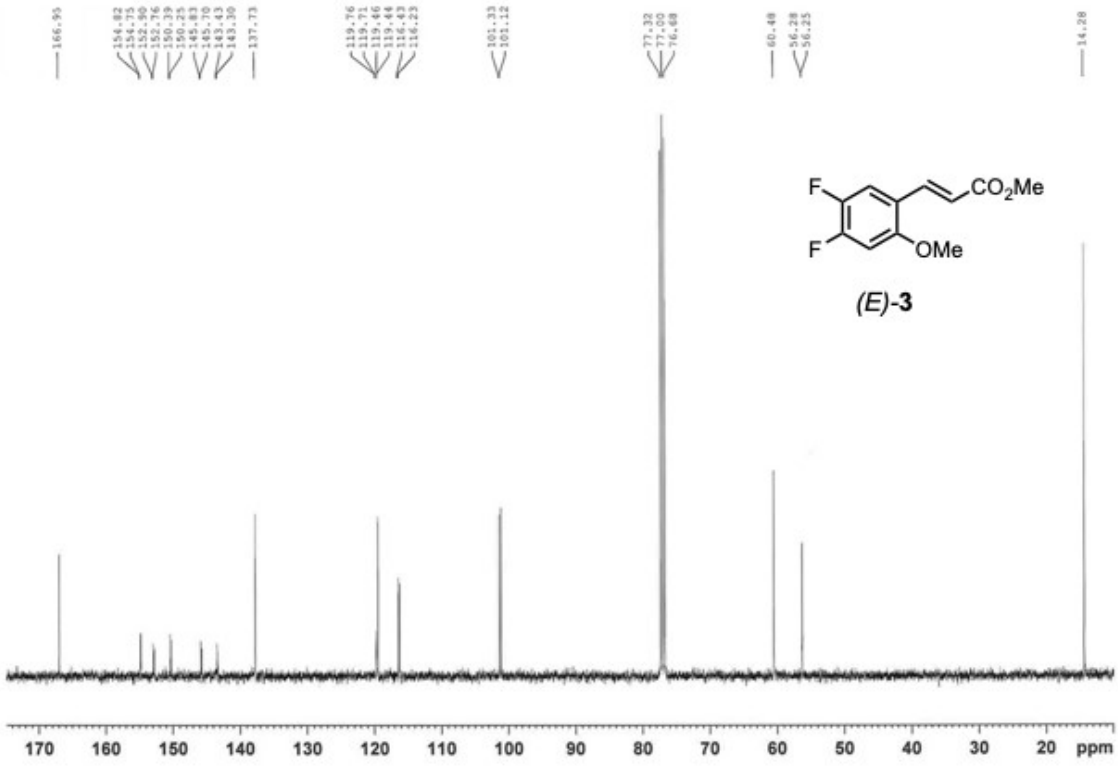

Figure S8. ^{13}C NMR spectrum of (*E*)-**3** ($CDCl_3$, 100 MHz).

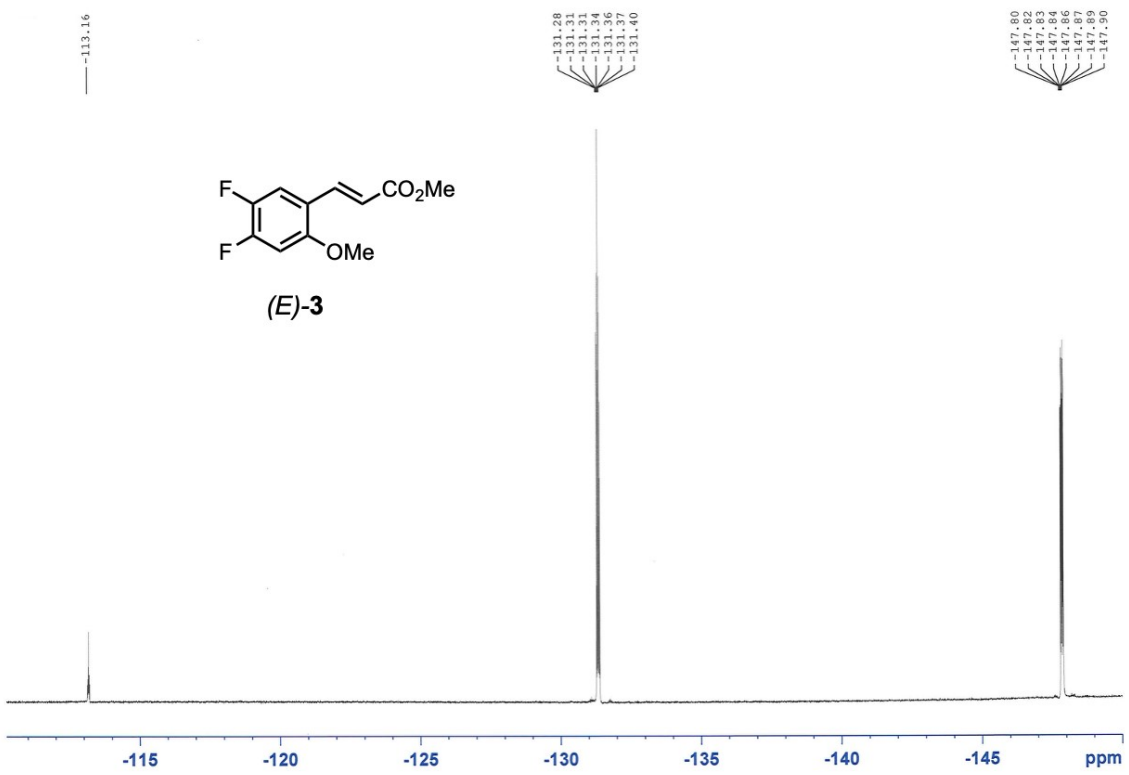

Figure S9. ^{19}F NMR spectrum of (*E*)-**3** ($CDCl_3$ with C_6H_5F, 376 MHz)

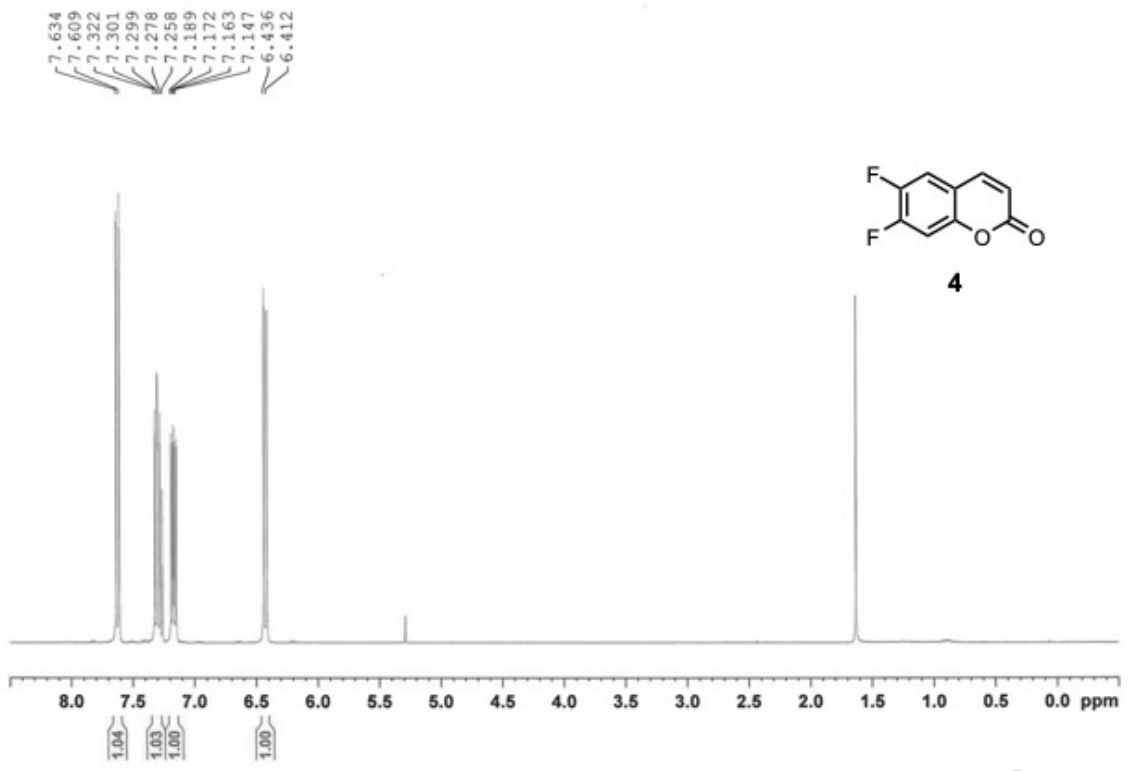

Figure S10. ^{1}H NMR spectrum of **4** ($CDCl_3$, 400 MHz).

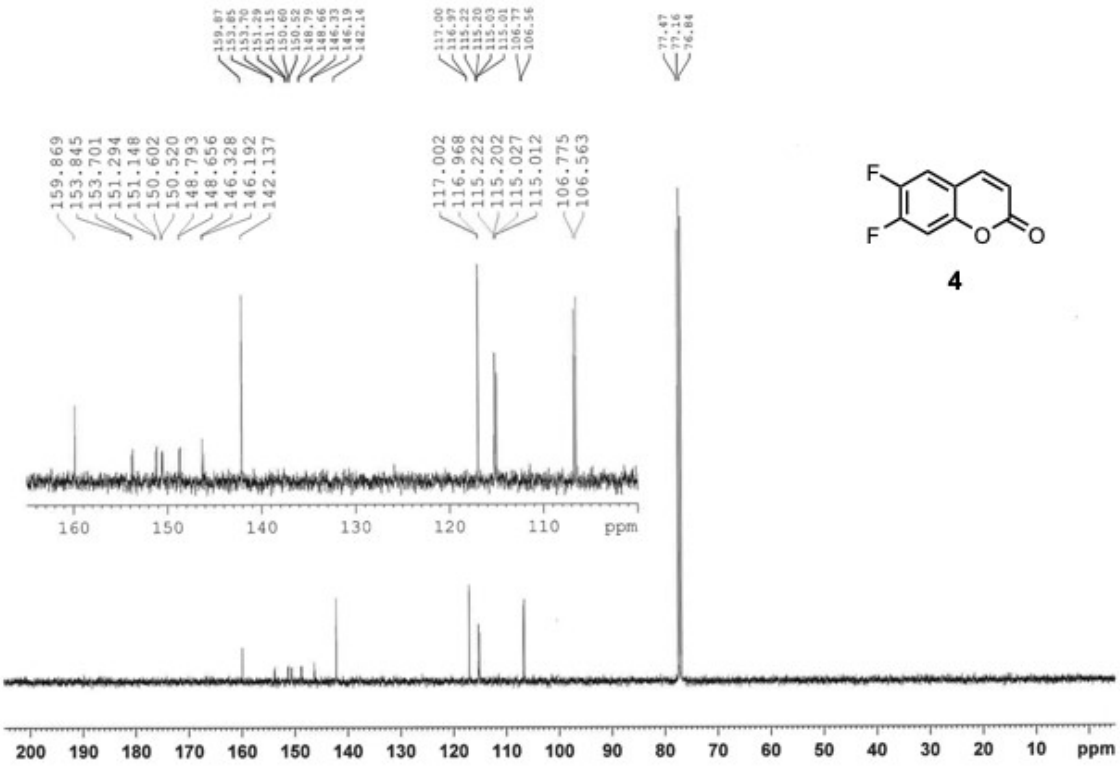

Figure S11. ^{13}C NMR spectrum of **4** ($CDCl_3$, 100 MHz).

Figure S12. ^{19}F NMR spectrum of **4** ($CDCl_3$ with C_6H_5F, 376 MHz).

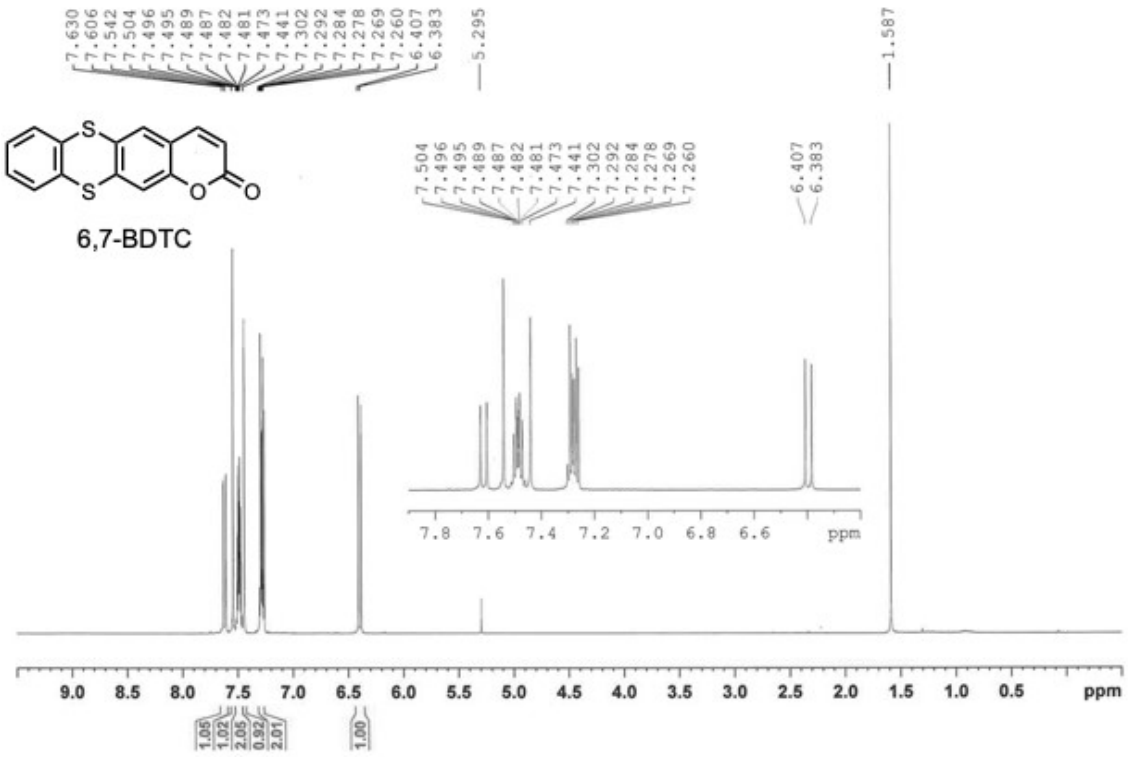

Figure S13. ^{1}H NMR spectrum of 6,7-BDTC ($CDCl_3$, 400 MHz).

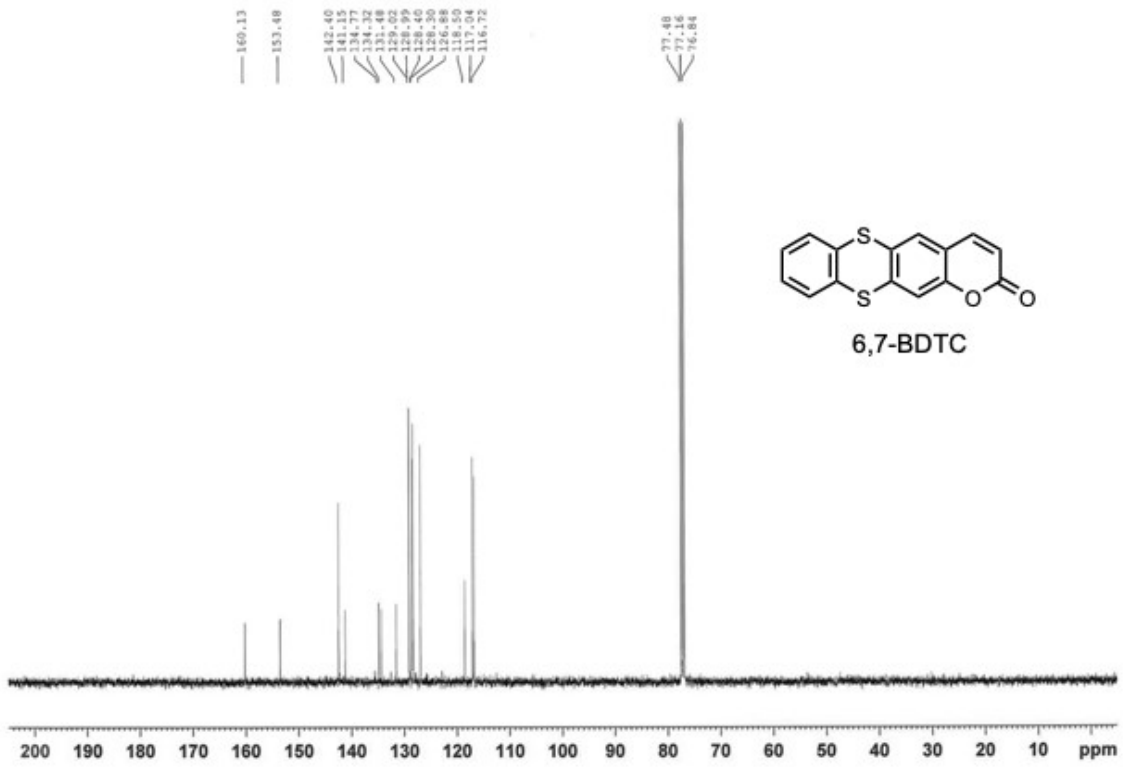

Figure S14. ^{13}C NMR spectrum of 6,7-BDTC ($CDCl_3$, 100 MHz).

3. HRMS Spectrometry Data

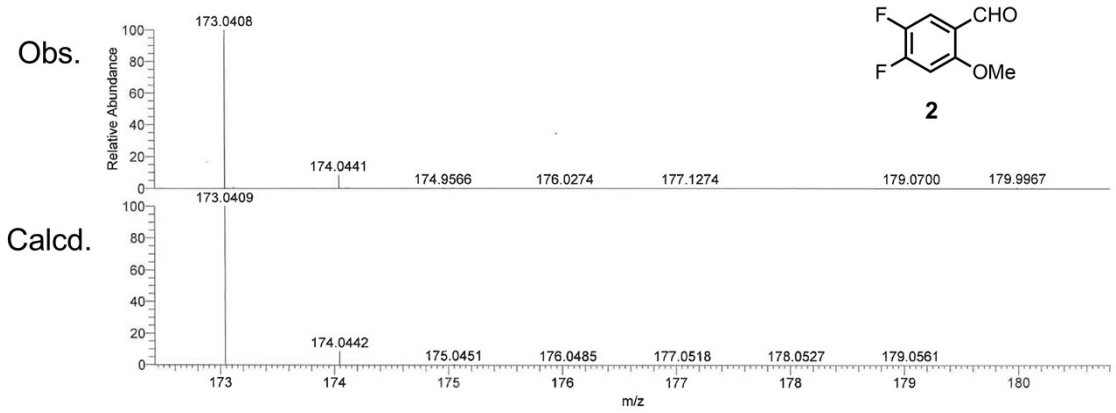

Figure S15. ESI-MS spectrum of **2**.

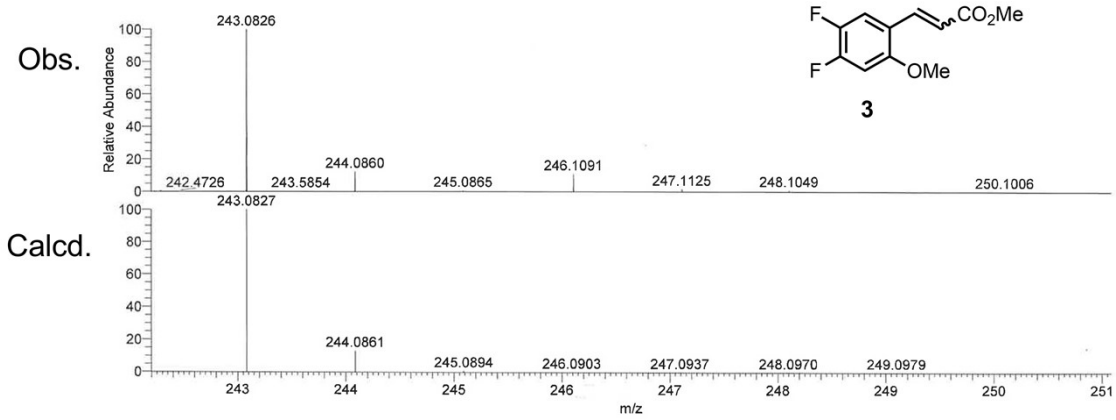

Figure S16. ESI-MS spectrum of **3**.

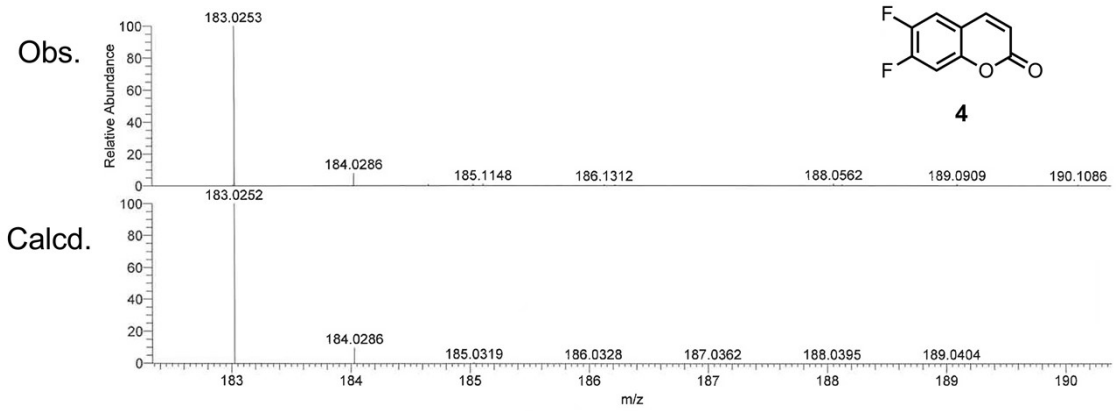

Figure S17. ESI-MS spectrum of **4**.

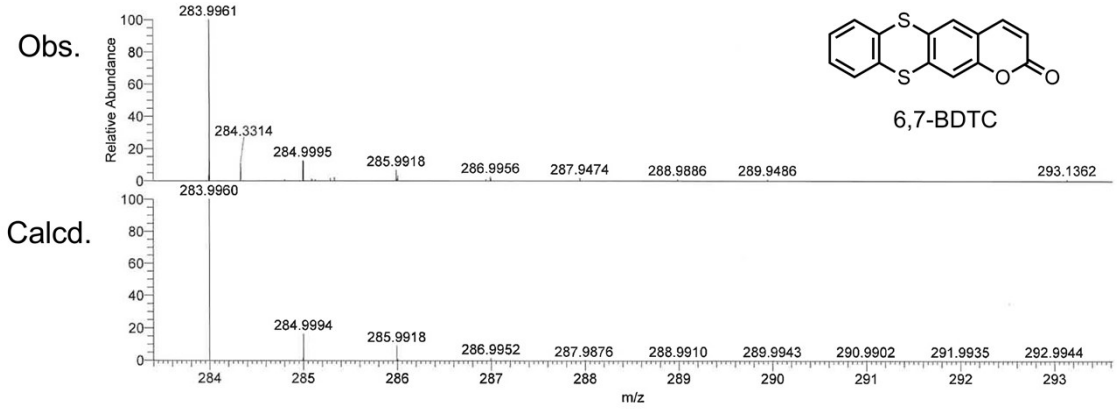

Figure S18. ESI-MS spectrum of 6.7-BDTC.

4. Optical Properties

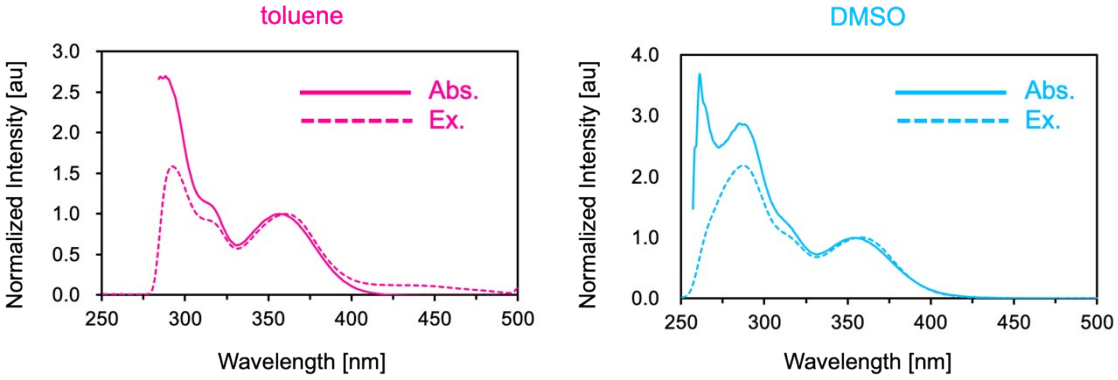

Figure S19. Normalized absorption and excitation spectra of 6,7-BDTC in toluene (left) and DMSO (right).

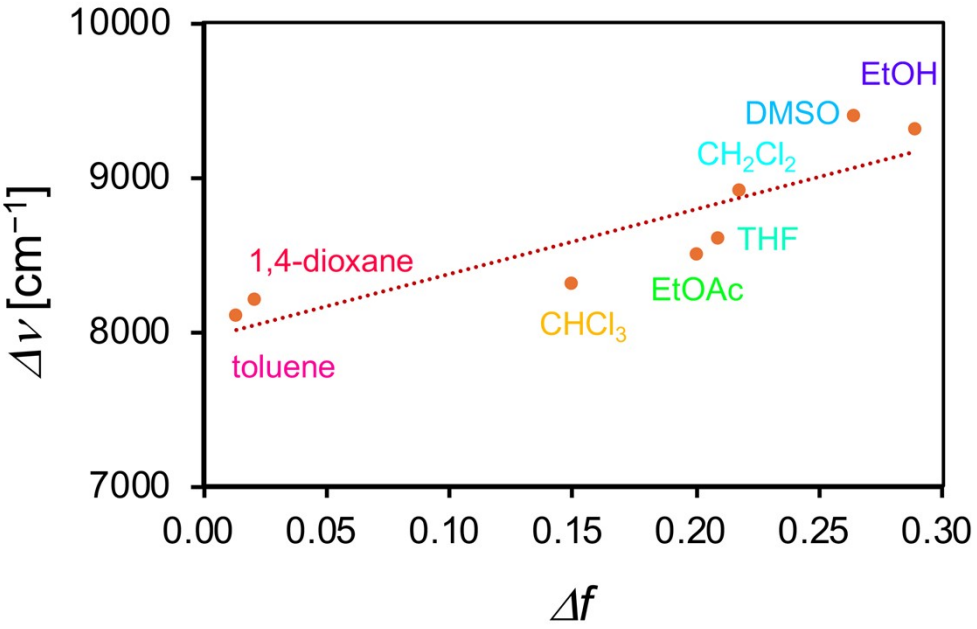

Figure S20. Lippert-Mataga plot for 6,7-BDTC in tested solvents. $\Delta\nu = \nu_{abs} - \nu_{fluo}$, $\Delta f = (\varepsilon_r - 1/2\varepsilon_r + 1) - (n^2 - 1/2n^2 + 1)$. ε = solvent dielectric constant, n = refractive index.

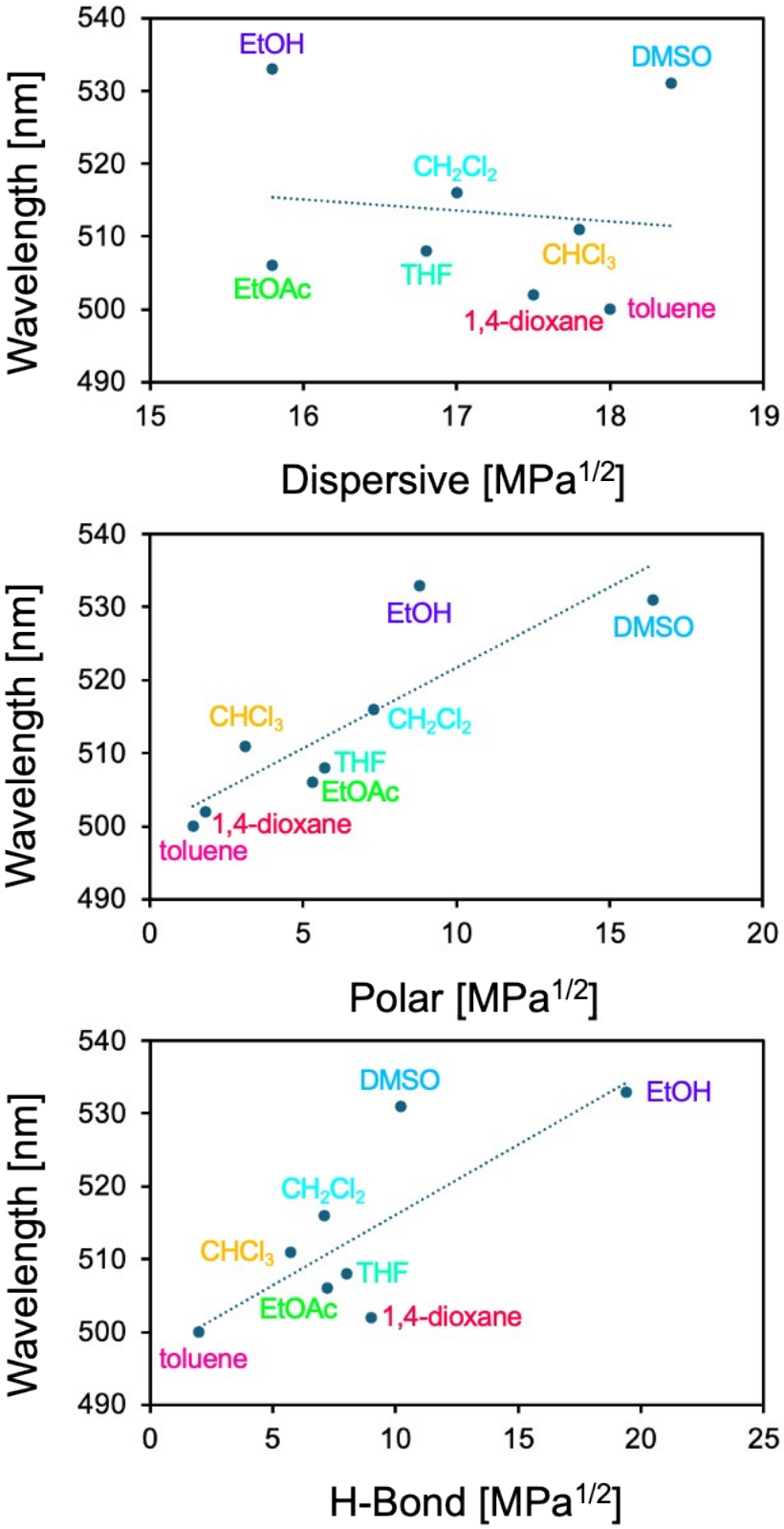

Figure S21. The linear correlations between emission wavelengths and Hansen solubility parameters of 6,7-BDTC in the tested solvents.

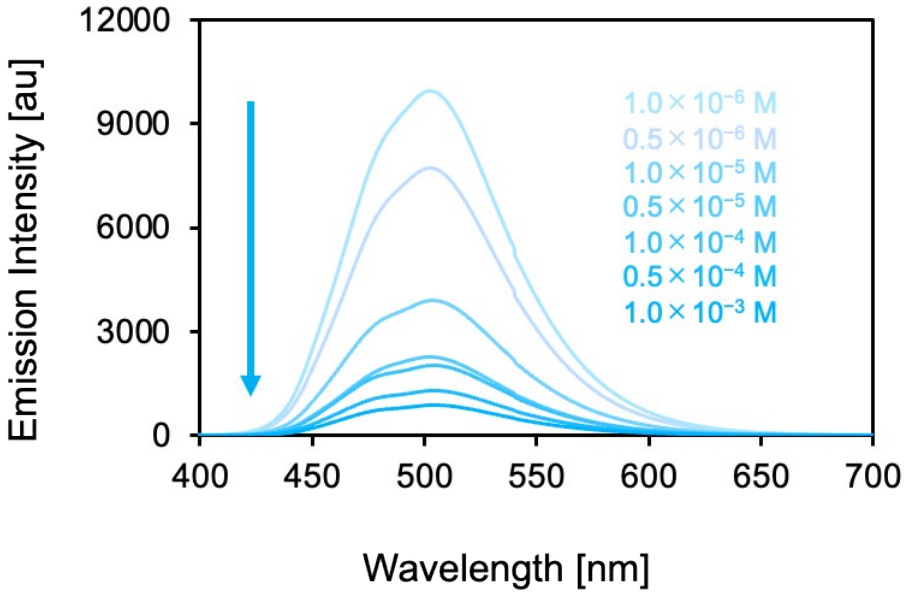

Figure S22. Emission Spectra of different concentrations of 6,7-BDTC in 1,4-dioaxane.

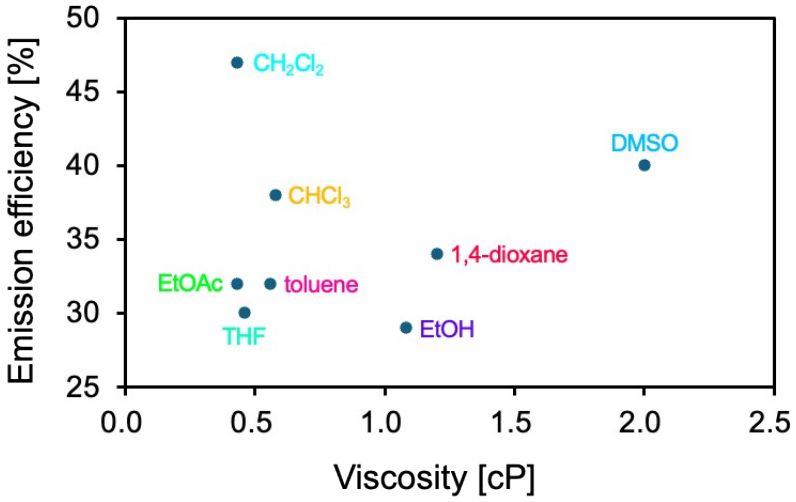

Figure S23. Dependence of emission efficiency on the solvent viscosity.

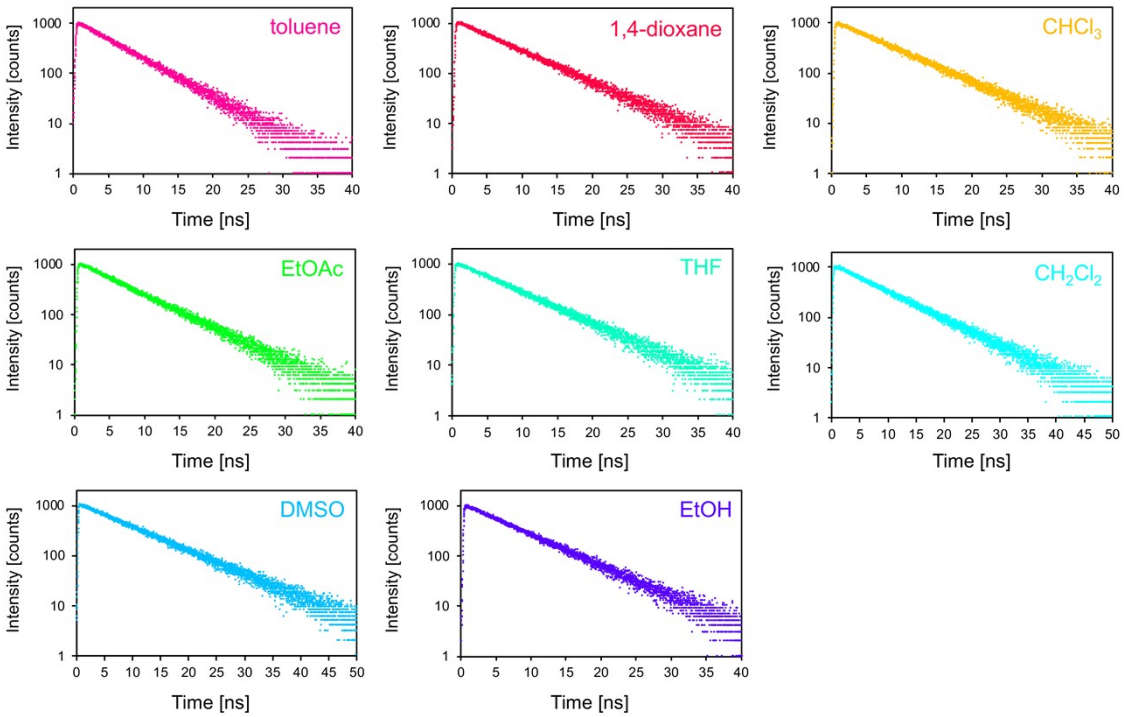

Figure S24. Fluorescence decay of 6,7-BDTC in the tested solvents.

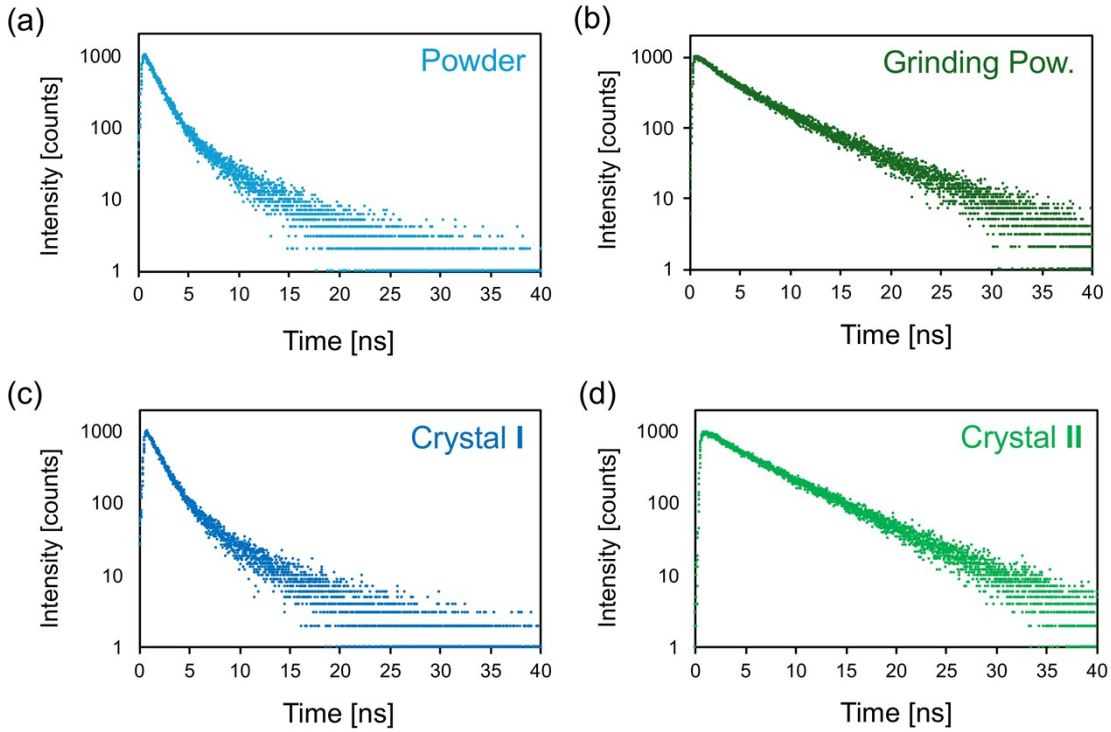

Figure S25. Fluorescence decay of 6,7-BDTC in the solid state: (a) powder; (b) grinding powder; (c) crystal **I**; (d) crystal **II**.

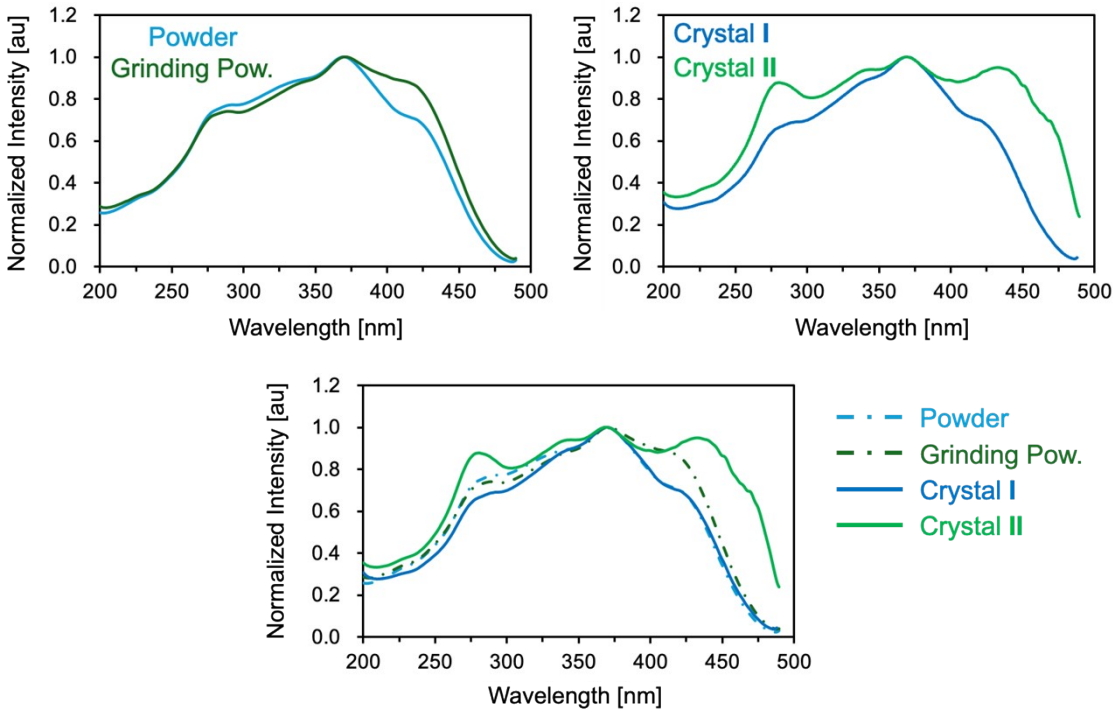

Figure S26. Normalized excitation spectra of 6,7-BDTC in the solid state.

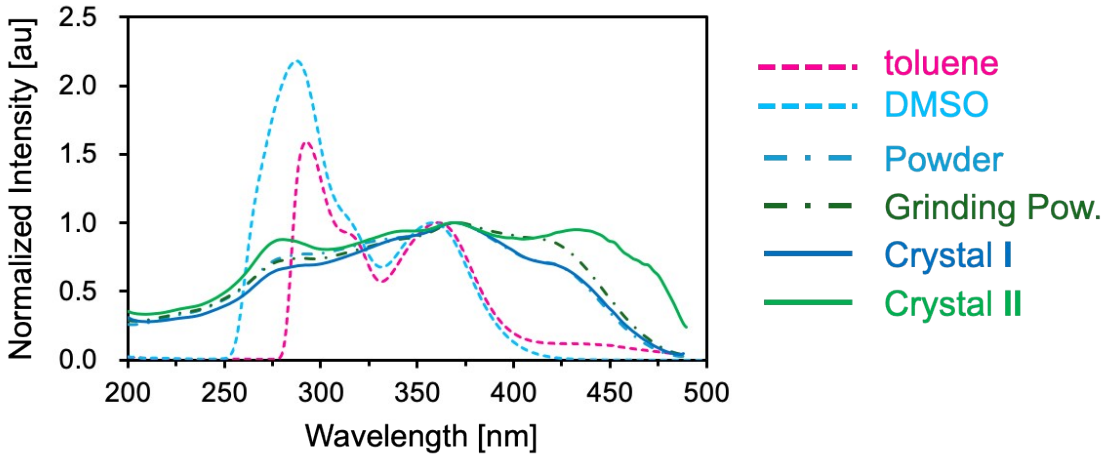

Figure S27. Normalized excitation spectra of 6,7-BDTC in solutions, powders and crystals.

Table S1. Information on fluorescence decay analysis for 6,7-BDTC.

State	Detection [nm]	Reaction order		τ [ns]	Rel. Ampl [%]	Ave. τ [ns]	X^2
toluene	500	1st	τ_1	5.70	-	-	1.166
1,4-dioxane	502	1st	τ_1	6.97	-	-	1.109
$CHCl_3$	511	1st	τ_1	7.14	-	-	1.111
EtOAc	506	1st	τ_1	6.48	-	-	1.147
THF	508	1st	τ_1	7.07	-	-	1.189
CH_2Cl_2	516	1st	τ_1	8.08	-	-	1.001
DMSO	531	1st	τ_1	9.12	-	-	1.053
EtOH	533	1st	τ_1	7.00	-	-	1.090
Powder	513	2nd	τ_1	1.45	73.8	2.51	1.040
			τ_2	5.49	26.2		
Grind. Pow.	513	2nd	τ_1	2.67	26.4	5.75	1.185
			τ_2	6.86	73.6		
Crystal I	504	2nd	τ_1	1.50	71.0	2.61	1.080
			τ_2	5.33	29.0		
Crystal II	511	1st	τ_1	6.60	-	-	1.245

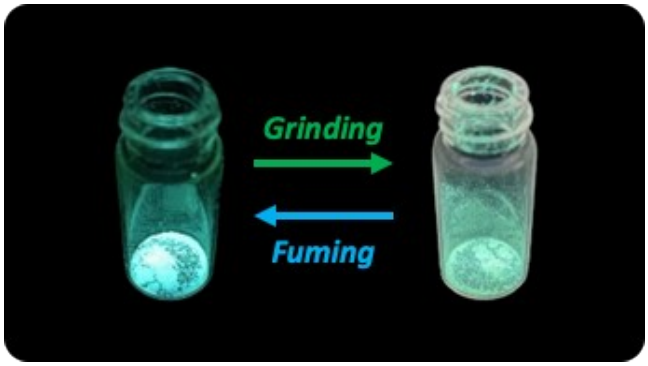

Figure S28. Photographic images of fumed (CH_2Cl_2 vapor) and ground samples of 6,7-BDTC under irradiation by a 365 nm UV lamp.

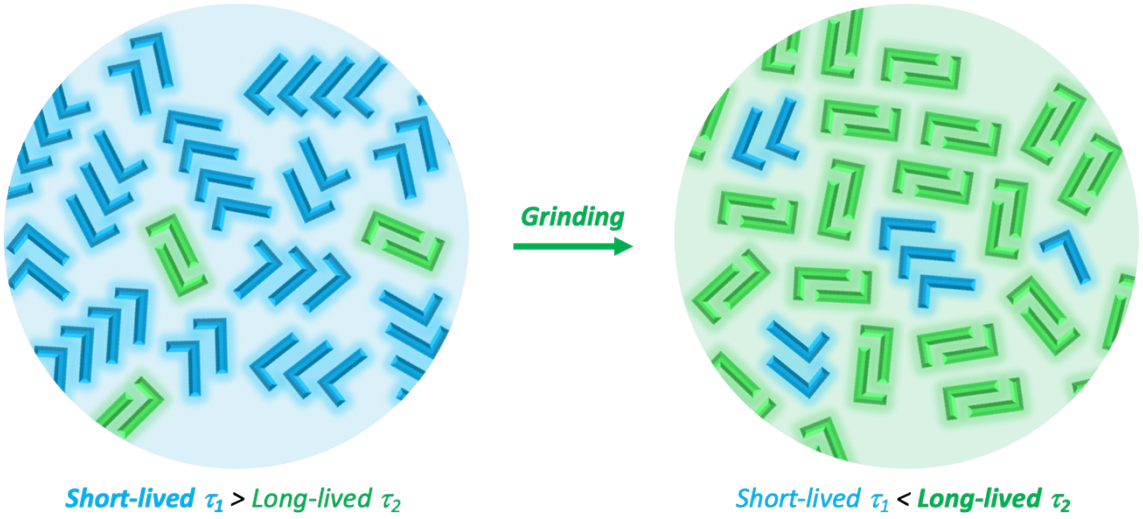

Figure S29. Schematic illustration of mechanochromic behavior of 6,7-BDTC in powder.

5. Crystal Data and Crystal Structures

Table S2. Crystal data of Crystal **I** and **II** for 6,7-BDTC.

Crystals	Crystal **I**	Crystal **II**
Formula	$C_{15}H_8O_2S_2$	$C_{15}H_8O_2S_2$
T [K]	100.15	100.15
Crystal system	monoclinic	monoclinic
Space group	*I*2/a	$P2_1/n$
a [Å]	13.5461(3)	6.8001(2)
b [Å]	3.86020(10)	14.5918(5)
c [Å]	46.3601(9)	12.0415(4)
α [deg.]	90	90
β [deg.]	95.505(2)	94.287(3)
γ [deg.]	90	90
V [Å^3]	2413.02(9)	1191.48(7)
Z	8	4
D_{calc} [gcm^{-3}]	1.565	1.585
μ [mm^{-1}]	3.946	3.996
F (000)	1168.0	584.0
Reflection collected	7033	7662
Parameters	172	172
Goodness-of-fit on F^2	1.043	1.097
*R*1/*wR*2 [$I>2\sigma(I)$]	0.0329/0.0862	0.0438/0.1282
*R*1/*wR*2 [all data]	0.0342/0.0873	0.0470/0.1306
CCDC number	2487912	2487913

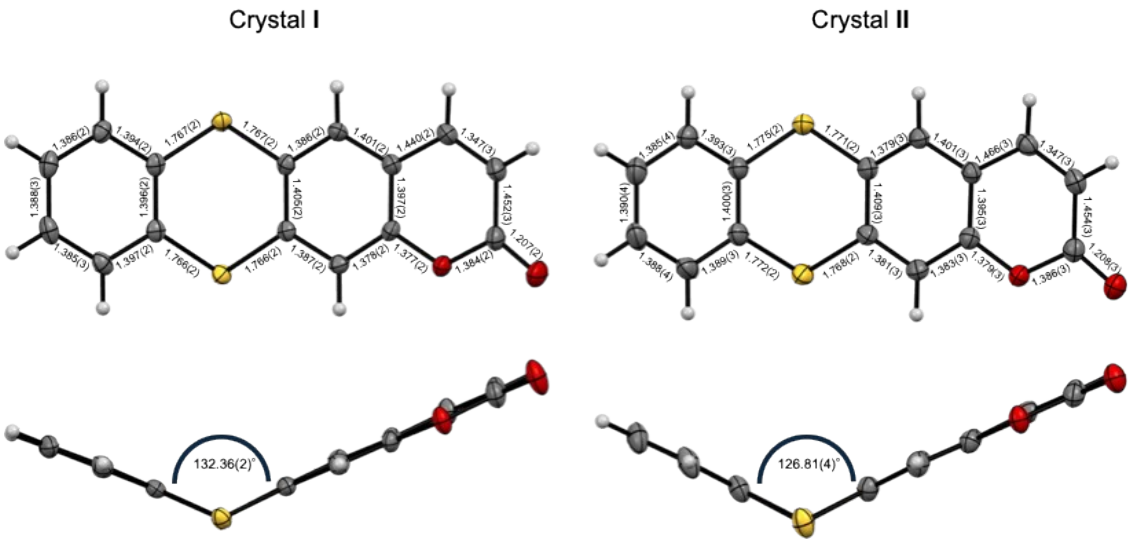

Figure S30. Molecular structures of 6,7-BDTC in Crystal **I** and **II**. The values in the figure indicate the bond lengths [Å] and the dihedral angle. The ellipsoids indicate a 50% probability of formation.

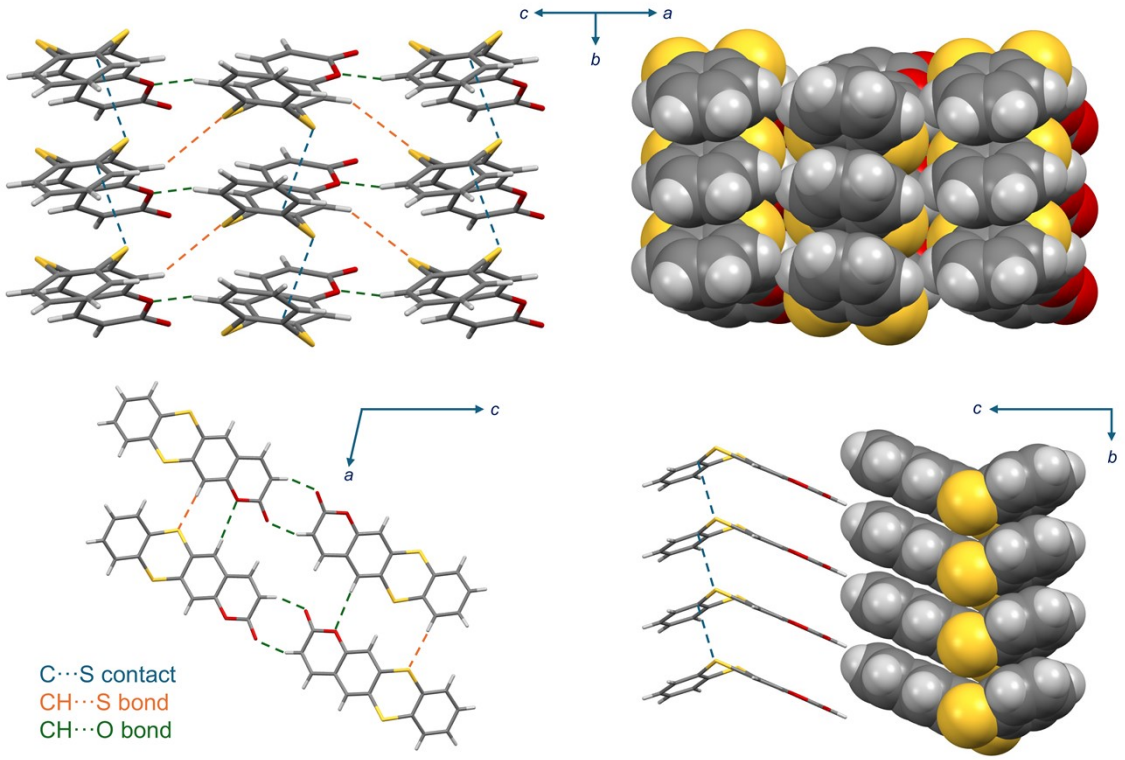

Figure S31. Crystal structure of 6,7-BDTC in Crystal **I**.

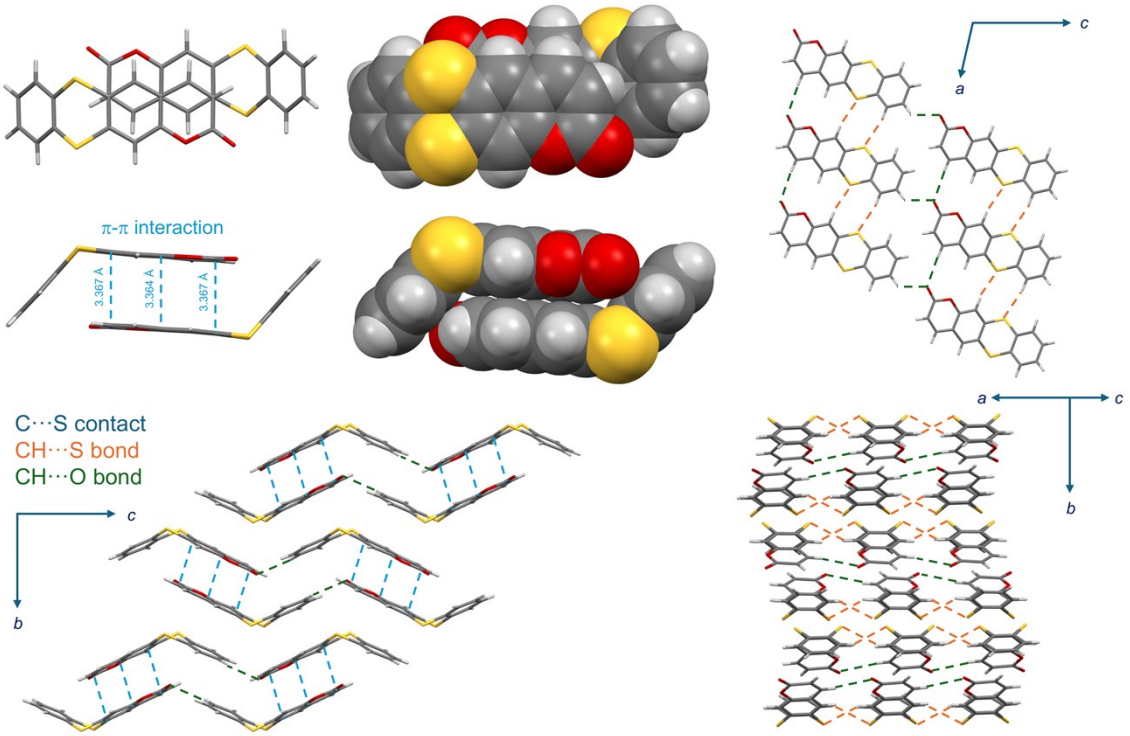

Figure S32. Crystal structure of 6,7-BDTC in Crystal **II**.

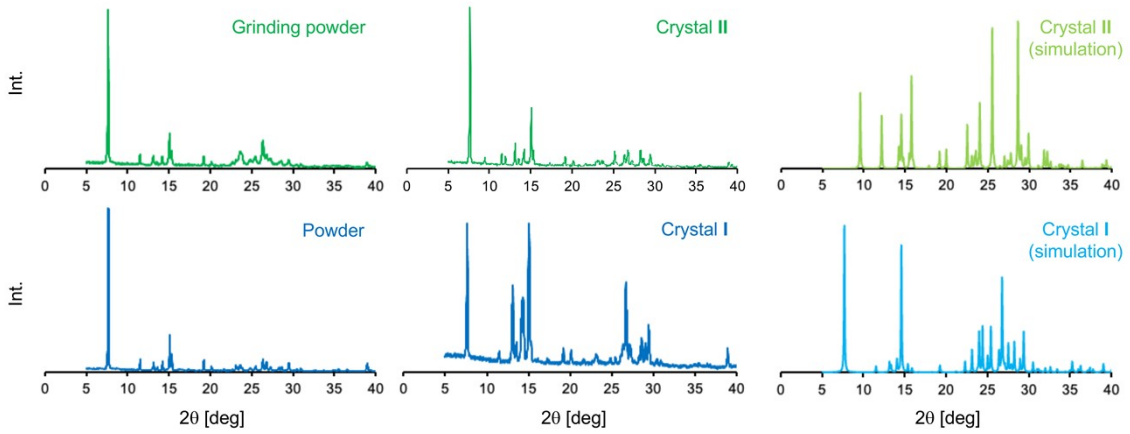

Figure S33. XRD patterns of 6,7-BDTC in the solid state (powder, grinding powder, crystal **I**, and **II**) and these simulation patterns of crystals.

6. Theoretical Study

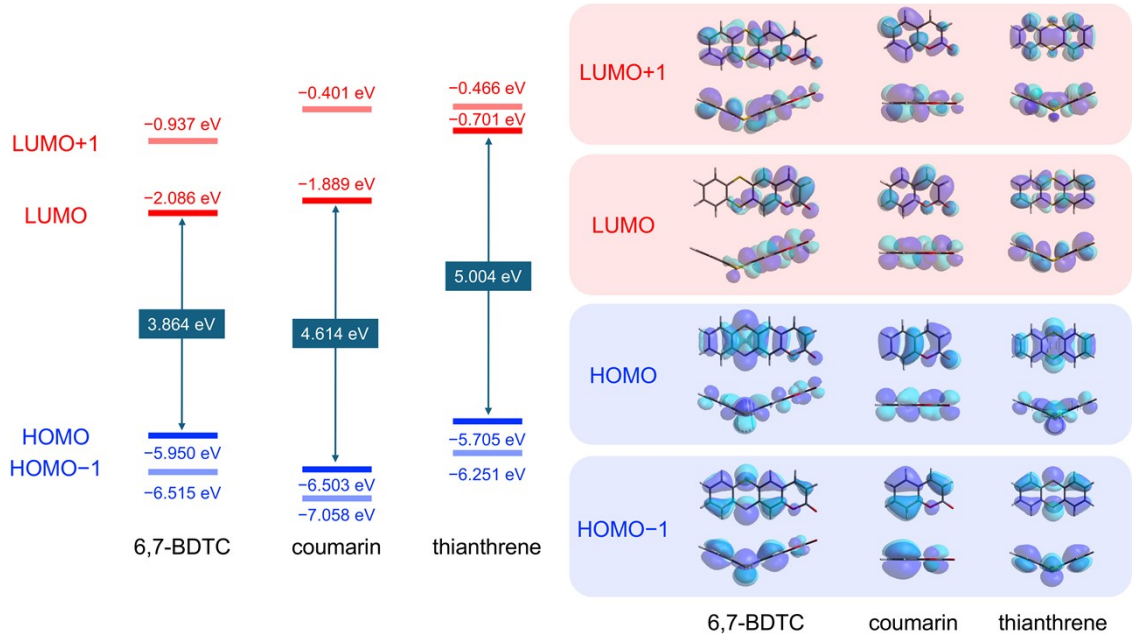

Figure S34. Selected molecular orbitals of 6,7-BDTC, coumarin, and thianthrene.

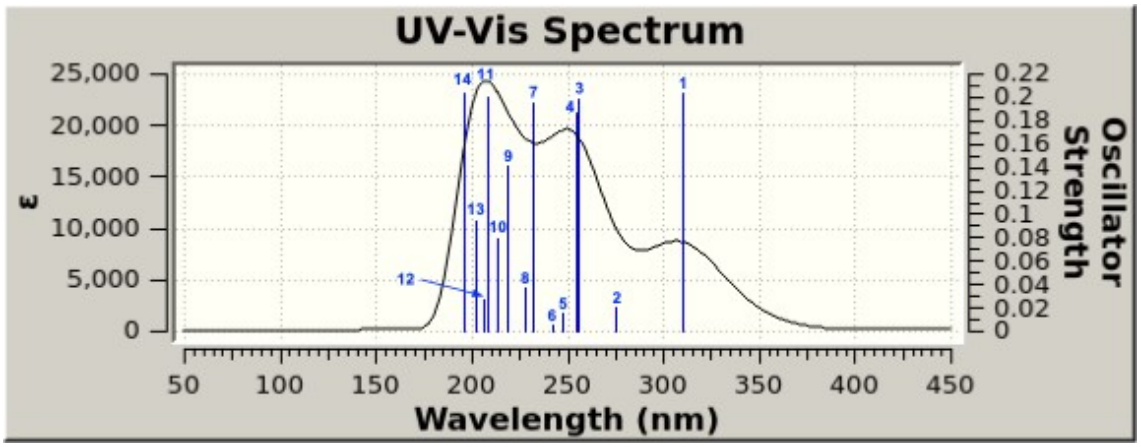

Figure S35. Theoretical absorption spectra of 6,7-BDTC.

Table S3. Summary of TDDFT calculation of 6,7-BDTC. (H: HOMO; L: LUMO)

Electronic transition	Energy [eV]	Energy [nm]	Oscillator strength	Composition	CI coefficients
1: $S_0 \rightarrow S_1$	4.0039	309.65	0.2027	H−3 → L (5%)	0.16194
				H → L (84%)	0.64906
2: $S_0 \rightarrow S_2$	4.5086	275.00	0.0205	H−3 → L (6%)	−0.18070
				H−2 → L (2%)	−0.10007
				H−1 → L (41%)	0.45517
				H → L+1 (39%)	0.44183
3: $S_0 \rightarrow S_3$	4.8459	255.86	0.1979	H−4 → L (32%)	0.40083
				H−4 → L+4 (6%)	−0.17071
				H−2 → L+1 (2%)	0.10249
				H−1 → L (19%)	0.30507
				H → L+1 (25%)	−0.35446
				H → L+2 (2%)	−0.10013
4: $S_0 \rightarrow S_4$	4.8664	254.77	0.1871	H−4 → L (43%)	0.46526
				H−4 → L+4 (8%)	−0.19825
				H−3 → L (2%)	0.11091
				H−2 → L (9%)	−0.21483
				H−1 → L (12%)	−0.24686
				H → L+1 (11%)	0.23462
				H → L+2 (3%)	0.11323
5: $S_0 \rightarrow S_5$	5.0212	246.92	0.0145	H−3 → L+1 (4%)	0.13913
				H−3 → L+2 (2%)	0.11090
				H−2 → L (18%)	−0.30178
				H−2 → L+2 (3%)	−0.12262
				H−2 → L+3 (7%)	0.18923
				H−1 → L+1 (11%)	0.23572
				H−1 → L+2 (4%)	0.13909
				H → L+1 (3%)	−0.11242
				H → L+2 (23%)	0.33567
				H → L+3 (15%)	−0.27467
6: $S_0 \rightarrow S_6$	5.1227	242.03	0.0042	H−5 → L (3%)	0.11534
				H−3 → L+1 (2%)	0.10203
				H−2 → L (45%)	0.47598
				H−2 → L+2 (3%)	−0.11545
				H → L (4%)	−0.13755
				H → L+1 (5%)	0.15156
				H → L+2 (3%)	0.12833
				H → L+3 (13%)	−0.26256
				H → L+4 (6%)	−0.17632
				H → L+5 (2%)	0.11120
7: $S_0 \rightarrow S_7$	5.3366	232.33	0.1954	H−2 → L (6%)	0.17547
				H−1 → L+1 (16%)	0.28056
				H−1 → L+7 (3%)	0.12204

				H → L+2 (11%)	0.23290
				H → L+3 (28%)	0.37522
				H → L+5 (19%)	−0.30585
8: $S_0 \rightarrow S_8$	5.4342	228.15	0.0361	H−1 → L (16%)	−0.28336
				H−1 → L+1 (26%)	0.36376
				H → L+1 (2%)	0.10657
				H → L+2 (25%)	−0.35490
				H → L+3 (3%)	−0.12880
				H → L+4 (4%)	−0.14230
				H → L+5 (8%)	−0.19740
9: $S_0 \rightarrow S_9$	5.6609	219.02	0.1411	H−6 → L (3%)	−0.13117
				H−3 → L (16%)	0.28438
				H−2 → L+2 (3%)	0.11800
				H−1 → L+1 (3%)	−0.11799
				H−1 → L+2 (19%)	0.30785
				H → L (2%)	−0.10274
				H → L+2 (14%)	−0.26297
				H → L+3 (3%)	−0.13017
				H → L+4 (11%)	0.23024
				H → L+5 (6%)	−0.17106
10: $S_0 \rightarrow S_{10}$	5.8089	213.44	0.0795	H−6 → L (6%)	−0.17260
				H−3 → L (30%)	0.39021
				H−2 → L+1 (4%)	−0.13245
				H−1 → L (3%)	0.11937
				H−1 → L+1 (11%)	0.23127
				H−1 → L+4 (2%)	0.10259
				H → L+4 (9%)	−0.20917
				H → L+5 (22%)	0.33101
11: $S_0 \rightarrow S_{11}$	5.9495	208.40	0.2007	H−3 → L (10%)	−0.22049
				H−1 → L+1 (8%)	0.20415
				H−1 → L+2 (12%)	0.24366
				H−1 → L+3 (11%)	0.23970
				H−1 → L+4 (3%)	−0.12922
				H → L+2 (4%)	−0.13708
				H → L+3 (10%)	0.22602
				H → L+4 (7%)	0.18262
				H → L+5 (21%)	0.32170
12: $S_0 \rightarrow S_{12}$	6.0233	205.84	0.0276	H−2 → L+1 (4%)	0.14313
				H−1 → L+2 (25%)	0.35695
				H−1 → L+3 (21%)	−0.32543
				H−1 → L+5 (17%)	0.29316
				H → L+1 (5%)	0.15828
				H → L+3 (6%)	0.17501
				H → L+7 (6%)	−0.16859
13: $S_0 \rightarrow S_{13}$	6.1367	202.04	0.0944	H−2 → L (3%)	0.12563
				H−2 → L+2 (2%)	0.10543

				H−2 → L+4 (3%)	0.11492
				H−1 → L+1 (11%)	0.22998
				H−1 → L+2 (6%)	−0.17497
				H−1 → L+3 (18%)	−0.29829
				H → L+3 (4%)	−0.14285
				H → L+4 (37%)	0.43222
				H → L+5 (3%)	0.11925
14: $S_0 \rightarrow S_{14}$	6.3148	196.34	0.2035	H−3 → L (5%)	0.15486
				H−2 → L+1 (43%)	0.46625
				H−2 → L+2 (11%)	−0.23783
				H−2 → L+3 (9%)	−0.21339
				H−1 → L+3 (4%)	0.14114
				H−1 → L+4 (14%)	0.26700

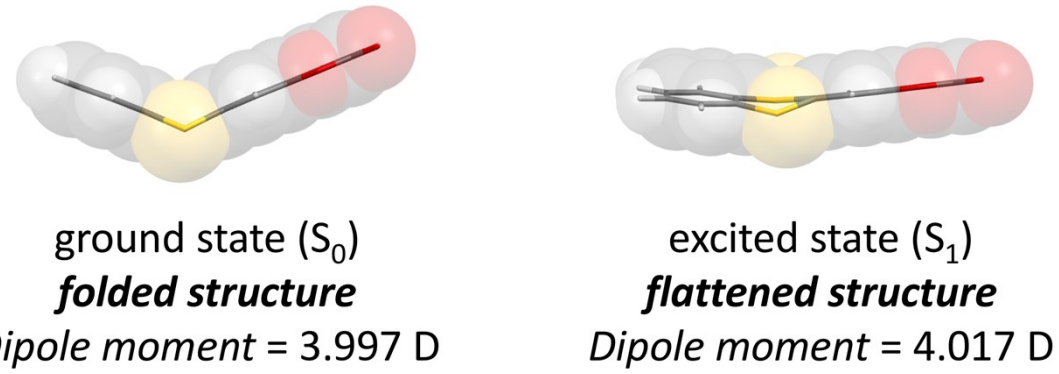

Figure S36. Optimized structures of 6,7-BDTC in its ground (S_0) and excited state (S_1).

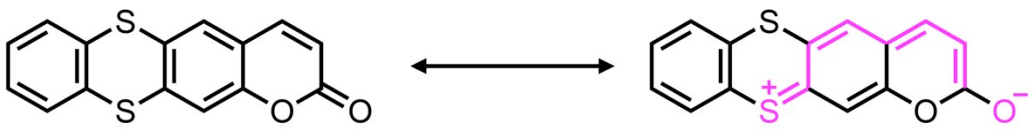

Figure S37. Resonance structures of 6,7-BDTC.